THE JOURNAL OF PHYSICAL CHEMISTRY C
A JOURNAL OF THE AMERICAN CHEMICAL SOCIETY

pubs.acs.org/JPCC

Article

Angular Distribution Analysis of Permanent Dipole Moments in Amorphous Organic Semiconductor Film with Large Spontaneous Orientation Polarization

Yuro Yagi, Yutaka Noguchi, and Daisuke Yokoyama*

Cite This: J. Phys. Chem. C 2024, 128, 6072−6079

Read Online

ACCESS | Metrics & More | Article Recommendations | Supporting Information

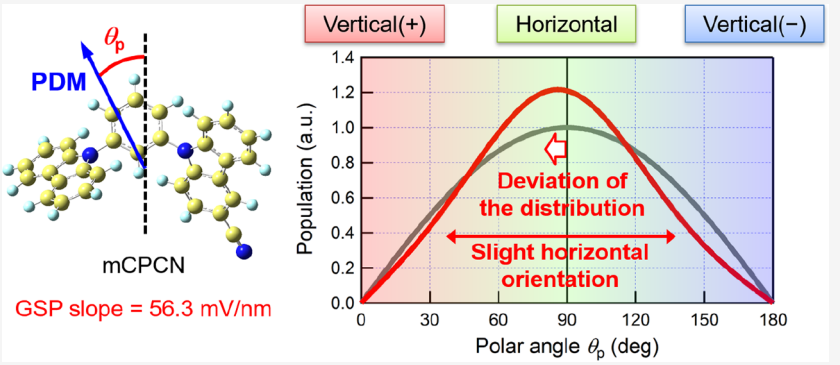

ABSTRACT: Spontaneous orientation polarization (SOP) in vacuum-deposited amorphous organic films occurs when molecular permanent dipole moments (PDMs) are anisotropically oriented. This phenomenon has recently been observed in many types of organic light-emitting diode (OLED) materials as a factor significantly affecting device performance. Although the formation mechanism of SOP can be explained in terms of surface equilibration, quantitative estimation of SOP based on molecular structure remains challenging, partly because the information on PDM angular distribution is lacking. In this study, we analyzed the PDM angular distribution in vacuum-deposited amorphous films of a commonly used host material 9-(3-(9*H*-carbazol-9-yl)phenyl)-9*H*-carbazole-3-carbonitrile (mCPCN). Defining θ_p as the angle between the PDM and surface normal, we estimated the average and variance of cos θ_p, $\langle \cos \theta_p \rangle$ and $V_{\cos \theta_p}$, respectively, based on Kelvin probe, X-ray reflectometry, impedance, and IR absorption measurements, and uniquely determined the angular distribution of θ_p assuming a normal distribution of cos θ_p. A very slight deviation in the angular distribution from random distribution resulted in the large SOP of the mCPCN films. Our angular distribution analysis method, based on obtaining $\langle \cos \theta_p \rangle$ and $V_{\cos \theta_p}$, can be adopted generally to allow visualization of PDM angular distributions of OLED materials, leading to further understanding of the formation mechanism of large SOP.

1. INTRODUCTION

Molecular orientation has recently become known as one of the key factors affecting the optical and electrical properties of vacuum-deposited amorphous organic semiconductor films and the organic light-emitting diodes (OLEDs) fabricated using these films. Since the generality of the molecular orientation of OLED materials was established, the positive effects of the horizontal orientation of emissive transition dipole moments (TDMs) and π-electron systems on the optical and electrical properties of OLEDs have been investigated and discussed.[1] Based on a considerable body of research into molecular orientation and its effects on OLED performance,[1−5] the importance of molecular orientation in OLEDs is now widely recognized, and the mechanism explaining its occurrence has been established.

On the other hand, the phenomenon of spontaneous orientation polarization (SOP),[6,7] which was first observed in organic semiconductors as a giant surface potential (GSP) on tris(8-hydroxyquinolate) aluminum (Alq_3) more than 20 years ago,[8] has also recently gained significant attention because it has also been observed in many types of OLED materials.[9,10] SOP occurs owing to the anisotropic orientation of molecular permanent dipole moments (PDMs) in a vacuum-deposited film, and the magnitude of the GSP is proportional to the film

Received: December 21, 2023
Revised: March 9, 2024
Accepted: March 11, 2024
Published: March 28, 2024

https://doi.org/10.1021/acs.jpcc.3c08315
J. Phys. Chem. C 2024, 128, 6072−6079

thickness and $\langle \cos \theta_p \rangle$, where θ_p is the angle between the PDM and surface normal, and $\langle \cdots \rangle$ indicates the ensemble average over the molecules in the film. Because SOP has been known to influence aspects of OLED device performance, including its charge injection,[11−13] accumulation,[14,15] efficiency,[16,17] and degradation[18−22] properties, PDM orientation and SOP are now considered as additional key factors for the maximization of OLED device performance.

The formation mechanisms of SOP in some specific materials, such as aluminum complexes including Alq_3,[7,23,24] iridium complexes including bis(2-phenylpyridine)-(acetylacetonate)iridium(III) [$Ir(ppy)_2(acac)$],[10,25,26] 1,3,5-tris(1-phenyl-1*H*-benzimidazol-2-yl)benzene (TPBi),[15,27] and trifluoromethyl materials,[28] have been investigated and discussed. Although the occurrence of the SOP phenomenon in commonly used OLED materials can generally be explained by the surface equilibration mechanism,[5,24,29] the molecular characteristics that determine the GSP magnitude in these OLED materials are still under discussion. Strong correlation between PDM orientation and PDM intensity, or between PDM and TDM orientations, has not been observed,[9,10] and thus predicting the GSP magnitude in the absence of electrical measurements or computational simulations remains challenging for commonly used OLED materials.

One of the reasons why the molecular characteristics associated with GSP remain unclear is the lack of information on angular distributions for PDMs. As mentioned above, the GSP magnitude is proportional to $\langle \cos \theta_p \rangle$, which can be estimated from experiments and chemical calculations, but $\langle \cos \theta_p \rangle$ is simply the average of the components of the PDMs projected onto the surface normal axis, and it does not include sufficient information on the entire PDM angular distribution. For example, $\langle \cos \theta_p \rangle = 0$ in three different extreme cases: (1) when the PDM orientations are completely isotropic (random), (2) when the PDM orientations are completely horizontal, and (3) when the PDM orientations are completely vertical, but the population is split equally between the top direction ["vertical(+)"] and bottom direction ["vertical(−)"]. Thus, even if $\langle \cos \theta_p \rangle$ is estimated, as an index of the GSP magnitude, it does not include information on the angular distribution of PDMs. The above-mentioned three extreme examples illustrate the fact that the mechanism whereby PDM orientation occurs should be significantly different depending on the angular distribution.

As an example, the PDM angular distributions of iridium complexes were investigated by Morgenstern et al.;[26] realistic possible angular distributions of the PDM orientation were estimated from experimentally determined PDM and TDM orientation factors Λ and Θ, respectively. However, because the directions of the PDM and TDM of these iridium complexes are quite different, the procedure required to associate the PDM and TDM orientations is complicated, and the PDM angular distribution was not unambiguously determined, though the upper limit of the width of the distribution was estimated for $Ir(ppy)_2(acac)$ doped in a host material. As another example, Friederich et al.[30] investigated the PDM angular distributions of some commonly used OLED materials using Monte Carlo simulations and identified short-range van der Waals interactions, rather than dipole interactions, as the main driving force of PDM orientation. However, these simulation results remain to be validated using experimental methods for the analysis of the PDM angular distribution.

In this study, we focused on a host material 9-(3-(9*H*-carbazol-9-yl)phenyl)-9*H*-carbazole-3-carbonitrile (mCPCN) (Figure 1) used in OLEDs, which exhibits large SOP in the form of a vacuum-deposited film, and we investigated the angular distribution characterizing the PDM orientation in mCPCN films. In recent years, emitting layers containing mCPCN have often been used in high-performance phosphorescent and thermally activated delayed fluorescent OLEDs.[31−35] Because the PDM of an mCPCN molecule corresponds principally to the polarity of its C≡N group, the directions of the C≡N bond and PDM are similar. We estimated $\langle \cos \theta_p \rangle$ based mainly on electrical measurements. Separately, based on IR absorption measurements, we estimated $\langle \cos^2 \theta_{CN} \rangle$, where θ_{CN} is the angle between the C≡N bond axis and surface normal. Taking advantage of the fact that $\langle \cos^2 \theta_{CN} \rangle$ is approximately equal to $\langle \cos^2 \theta_p \rangle$, we determined the variance of $\cos \theta_p$, $V_{\cos \theta_p}$, using the following statistical equation.

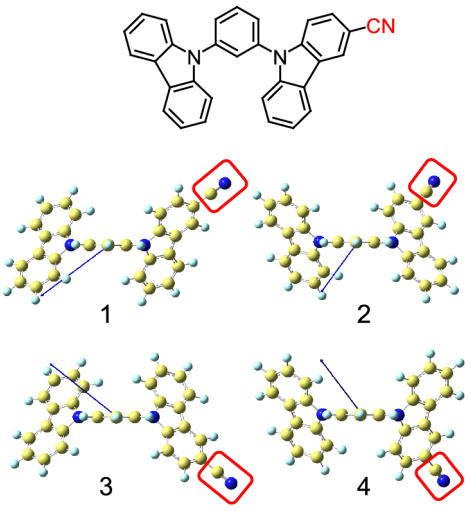

Figure 1. Chemical structure of mCPCN and optimized geometries of its four stable conformers, 1−4, obtained using molecular mechanics and DFT calculations. The blue arrows in the structures of the conformers are PDM vectors.

$$V_{\cos \theta_p} \equiv \langle (\cos \theta_p - \langle \cos \theta_p \rangle)^2 \rangle = \langle \cos^2 \theta_p \rangle - \langle \cos \theta_p \rangle^2 \quad (1)$$

Then, from the values of $\langle \cos \theta_p \rangle$ and $V_{\cos \theta_p}$, we uniquely determined the PDM angular distribution assuming a normal distribution of $\cos \theta_p$. By determining the average and variance of $\cos \theta_p$ for mCPCN molecules in a vacuum-deposited film, the angular distribution of its PDM orientation can be plotted, and this visually illustrates the fact that a very small deviation of the angular distribution from random distribution produces high-magnitude GSP in mCPCN films.

2. METHODS

2.1. Estimation of $\langle \cos \theta_p \rangle$. We determined $\langle \cos \theta_p \rangle$ from the following equation used for GSP calculations,[6,9,10]

$$V_s = \frac{dpn}{\varepsilon} \langle \cos \theta_p \rangle \quad (2)$$

where V_s is the surface potential, d is the film thickness, p is the PDM intensity, n is the molecular density, and ε is the

https://doi.org/10.1021/acs.jpcc.3c08315
J. Phys. Chem. C 2024, 128, 6072−6079

dielectric constant. To obtain the value of $\langle \cos \theta_p \rangle$, we separately estimated four factors: (1) p, via chemical calculations, (2) V_s/d, via Kelvin probe measurements, (3) n, via X-ray reflectometry (XRR) measurements, and (4) ε, via impedance measurements; the methods used for these estimations are described below in Sections 2.1.1−Sections 2.1.4, respectively.

Sublimation-grade mCPCN was purchased from Luminescence Technology Co. All the Si(100) and ITO glass substrates used were cleaned in advance with detergent, acetone, and 2-propanol and then dry-cleaned by UV−ozone exposure for 15 min. For each sample, the vacuum deposition of mCPCN was performed at a deposition rate of 2 Å/s under a vacuum of $<1 \times 10^{-4}$ Pa in the dark. The substrate temperature was not actively controlled, but it was monitored and remained at 25 ± 2 °C during the deposition of the film. Accurate thicknesses of mCPCN films were determined by means of variable angle spectroscopic ellipsometry analysis of mCPCN films simultaneously deposited on an Si substrate; an *M*-2000U variable angle spectroscopic ellipsometer and WVASE32 software (J. A. Woollam Co.) were used, and the ellipsometry data in the transparent range of 600−1000 nm were analyzed using a model in which the uniaxial anisotropy was added to the Cauchy model.

2.1.1. Chemical Calculations. A conformation search was performed for mCPCN using molecular mechanics calculations, implemented in the CONFLEX software package, with the MMFF94s force field. For each conformer, the optimized geometric structure, steric energy, PDM vector, and vibrational modes were obtained from density functional theory (DFT) calculations at the B3LYP/6-31G(d) level performed using Gaussian09 software.

2.1.2. Kelvin Probe Measurements. Films of mCPCN with thicknesses of ∼50, ∼100, and ∼200 nm were vacuum-deposited on one half of an ITO substrate. Without exposure to the atmosphere, the surface potential on the films on the ITO substrate was measured using the Kelvin probe method with a Trek 320C voltmeter and a 3250-V probe (Advanced Energy) under a vacuum of $\sim 1 \times 10^{-4}$ Pa in the dark. The surface potential on the films was measured as a function of the film thickness with reference to the ITO substrate. From the linear relationship between the surface potential and accurate thickness, the GSP slope V_s/d was determined.

2.1.3. XRR Measurements. An mCPCN film with a thickness of ∼100 nm was vacuum-deposited on an Si substrate. The XRR pattern of the mCPCN films on the Si substrate was measured using a SmartLab X-ray diffractometer (Rigaku Co.) under Cu Kα (λ = 1.54178 Å) radiation at 45 kV and 200 mA. The widths of the divergence, scattering, and receiving slits were 0.05, 0.1, and, 0.2 mm, respectively. The incident angle was scanned from 0° to 0.5° in steps of 0.004° at a scan rate of 0.1°/min. Fitting analysis of the XRR pattern was performed using GlobalFit software (Rigaku Co.) assuming a homogeneous film with a surface roughness. From the film density ρ, which was obtained from the XRR analysis, the molecular density n was determined using the expression

$$n = \frac{\rho N_A}{M} \tag{3}$$

where N_A is the Avogadro constant, and M is the molecular weight of mCPCN (433.5 g/mol).

2.1.4. Impedance Measurements. For impedance measurements, two devices with an area of 2.0 mm × 2.0 mm were fabricated on the ITO substrate. The structures of the two devices were glass/ITO (75 nm)/mCPCN (∼100 nm and ∼200 nm)/Al (100 nm). The impedance measurements were performed using an IM3570 impedance analyzer (Hioki E.E. Co.). The impedances of the devices were measured with a 200 mV AC voltage over frequencies of 10 Hz−1 MHz, without a DC bias voltage. Because carriers are not injected into the mCPCN film with such a low AC voltage, it was possible to determine the device capacitance C for each device using the expression

$$\mathrm{Im}\, Z = -\frac{1}{\omega C} \tag{4}$$

where Z is the complex impedance, and ω is the angular frequency of the AC voltage. At low frequencies, the capacitance of each device was constant at C_0. The static dielectric constant ε was determined from the expression

$$C_0 = \frac{\varepsilon S_D}{d_D} \tag{5}$$

where S_D is the device area, and d_D is the accurate thickness of the mCPCN film in the device.

2.2. Estimation of $\langle \cos^2 \theta_{CN} \rangle$. To estimate $\langle \cos^2 \theta_{CN} \rangle$, we performed IR-quantitative absorption comparison with an isotropically oriented standard (IR-QACIOS) measurement. The general method of QACIOS for orientation analysis is described in detail in previously published reports.[36,37] An mCPCN film with a thickness of ∼100 nm was deposited on an Si substrate, and its IR absorption spectrum was measured using an IRAffinity-1 Fourier-transform IR spectrometer (Shimadzu Co.). Then, the film was annealed for 10 min in a nitrogen atmosphere at 120 °C, which is a temperature sufficiently higher than the transition temperature, to ensure that it passed through the phase transition, and the molecules were randomly oriented. After cooling the sample, the IR absorption spectrum of this transition-experienced film was remeasured. Since the molecular orientation in the transition-experienced film is completely random, the orientation order parameter S for a TDM in the original as-deposited film can be determined from the ratio between the absorbance values measured before and after annealing:

$$S \equiv \frac{3\langle \cos^2 \theta_t \rangle - 1}{2} = 1 - \frac{A}{A_0} \tag{6}$$

where θ_t is the angle between the TDM and surface normal, A is the absorbance of the original as-deposited film, and A_0 is the absorbance of the transition-experienced film at the absorption peak assigned to the TDM.

In the IR absorption spectra of the mCPCN films, the band at 2220 cm^{-1} is assigned to the C≡N stretching vibrational mode, and the TDM of this vibrational mode (dipole derivative) is along the C≡N bond axis. Thus, we were able to determine $\langle \cos^2 \theta_{CN} \rangle$ using the expression

$$S_{CN} \equiv \frac{3\langle \cos^2 \theta_{CN} \rangle - 1}{2} = 1 - \frac{A_{CN}}{A_{0CN}} \tag{7}$$

where S_{CN} is the orientation order parameter of the C≡N bond, A_{CN} is the IR absorbance at 2220 cm^{-1} of the original as-deposited film, and A_{0CN} is that of the transition-experienced film.

https://doi.org/10.1021/acs.jpcc.3c08315
J. Phys. Chem. C 2024, 128, 6072−6079

3. RESULTS AND DISCUSSION

3.1. Estimation of $\langle \cos \theta_p \rangle$. The results of the molecular mechanics calculations indicated that the mCPCN molecule has four stable conformers. The optimized geometric structures of the four conformers and their PDMs, obtained by means of DFT calculations, are shown in Figure 1. Because the differences between the steric energies of the conformers are small (Table 1), all the conformers should be populated to

Table 1. Steric Energy Differences, Populations, and PDM Intensities of the Four Conformers 1−4.

conformer no.	steric energy difference (meV)	population (%)[a]	PDM intensity (debye)
1	0	32.8	6.19
2	2.5	29.7	6.81
3	14.1	18.9	6.30
4	14.5	18.6	6.88
weighted average			6.52

[a]Assumed to follow the Boltzmann distribution.

a certain extent in the vacuum-deposited amorphous films. The PDM intensities of the four conformers are similar (6−7 debye). Assuming that the populations of the conformers follow the Boltzmann distribution, we determined p as the weighted average of that of the four conformers; p = 6.52 debye.

Figure 2 shows the relationship between the surface potential and film thickness determined based on Kelvin

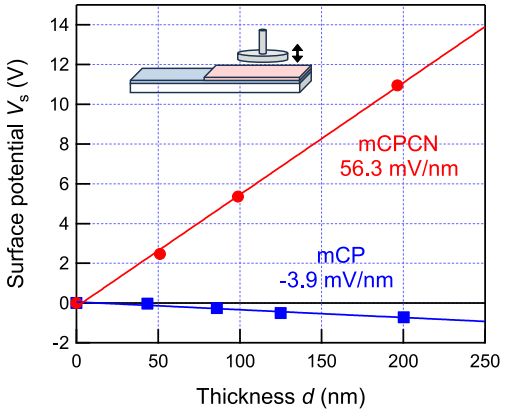

Figure 2. Surface potential of vacuum-deposited mCPCN films as a function of film thickness. For comparison, the corresponding data for mCP films[9] are also shown.

probe measurements. For comparison, the result for *N*,*N*-dicarbazolyl-3,5-benzene (mCP)[9] is also shown. At each thickness, although the magnitude of the surface potential is small for mCP, that for mCPCN is much larger, and a linear relationship between the surface potential and film thickness is apparent. From this result, we determined the GSP slope V_s/d of the mCPCN films; V_s/d = 56.3 mV/nm. This much larger GSP slope for mCPCN, compared to that of mCP, is attributed to the high polarity of the C≡N group, the orientation of which significantly affects the surface potential.

Figure 3 shows the experimental and calculated XRR patterns of the ∼100 nm-thick mCPCN film on the Si substrate. Through XRR analysis, assuming a homogeneous film with a surface roughness, the experimental XRR pattern is

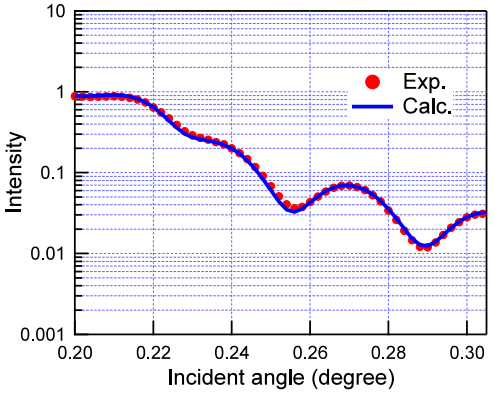

Figure 3. Experimental and calculated XRR patterns of the ∼100 nm-thick mCPCN film on the Si substrate.

well reproduced by the calculated one. The thickness, film density, and surface roughness were determined to be 102 nm, 1.22 g/cm^3, and 1.8 nm, respectively. From the obtained value of ρ = 1.22 g/cm^3, we determined n using eq 3; $n = 1.69 \times 10^{21}$ /cm^3.

Figure 4 shows the capacitances of the two devices obtained from the impedance measurements using eq 4. The accurate

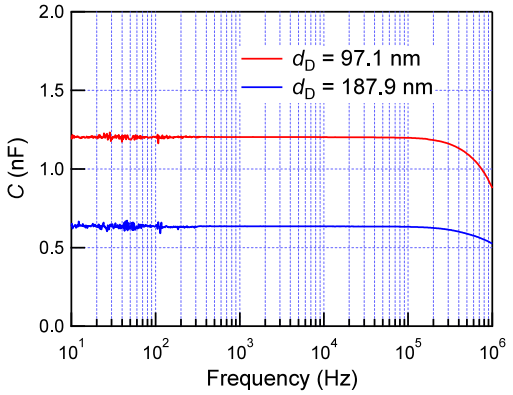

Figure 4. Capacitances of the two devices obtained from the impedance measurements.

thicknesses of the mCPCN film in the two devices were 97.1 and 187.9 nm, and the capacitances at low frequency, C_0, of the two devices were constant at 1.21 and 0.635 nF, respectively. From these results and the device structures, we determined the static dielectric constant ε using eq 5; $\varepsilon = 2.96 \times 10^{-11}$ F/m = 3.34 ε_0, where ε_0 is the vacuum dielectric constant.

Based on the above-discussed calculations and experiments, we obtained four factors for the estimation of $\langle \cos \theta_p \rangle$: p = 6.52 debye, V_s/d = 56.3 mV/nm, $n = 1.69 \times 10^{21}$ /cm^3, and $\varepsilon = 2.96 \times 10^{-11}$ F/m. Accordingly, using eq 2, we determined the average of cos θ_p; $\langle \cos \theta_p \rangle$ = 0.045.

3.2. Estimation of $\langle \cos^2 \theta_{CN} \rangle$. Figure 5 shows the IR absorption spectra of the mCPCN film before and after annealing in the spectral range of 1200−2300 cm^{-1}. There are many bands, each of which can be assigned to a vibrational mode of a functional group of mCPCN. The intensities of some peaks were slightly reduced after annealing, while those of other peaks were slightly greater. These results reflect the fact that the orientations of the TDMs (dipole derivatives) of some vibrational modes were changed from slightly horizontal to random after annealing, and those of other modes were

https://doi.org/10.1021/acs.jpcc.3c08315
J. Phys. Chem. C 2024, 128, 6072−6079

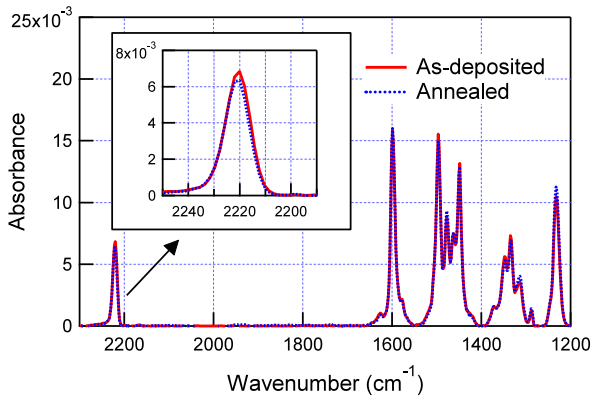

Figure 5. IR absorption spectra of the vacuum-deposited mCPCN film before and after annealing in the spectral range of 1200−2300 cm^{-1}. Inset: expanded view of the IR absorption band at 2220 cm^{-1} assigned to the C≡N stretching vibrational mode.

changed from slightly vertical to random; thus, the horizontal and vertical orientations of functional groups in the original as-deposited film can be analyzed.[37] In this study, we focused on the C≡N stretching vibrational mode, whose absorption band is isolated from the other bands at 2220 cm^{-1} (Figure 5, inset). The absorbance of this band was slightly decreased after annealing, indicating that the C≡ N bond in the original as-deposited film is slightly horizontally oriented. From the ratio of the absorbances before and after annealing, we determined S_{CN} and $\langle \cos^2 \theta_{CN} \rangle$ using eq 7; $S_{CN} = -0.08$ and $\langle \cos^2 \theta_{CN} \rangle = 0.28$, respectively.

3.3. Approximation of $\langle \cos^2 \theta_p \rangle$ as $\langle \cos^2 \theta_{CN} \rangle$. To experimentally estimate the variance of cos θ_p, we approximated $\langle \cos^2 \theta_p \rangle$ as $\langle \cos^2 \theta_{CN} \rangle$ because the PDM of the mCPCN molecule arises for the most part owing to the polarity of its C≡N group. However, θ_{CN} is not completely identical to θ_p. The directions of the PDM and C≡N bond differ slightly, and the angles between them in conformers 1−4 are 9°, 6°, 10°, and 6°, respectively. Therefore, to validate this approximation, we estimated the possible error arising from this difference in the angles.

Without loss of generality, the unit vector of the PDM, $\hat{\mathbf{p}}$, can be expressed as follows.

$$\hat{\mathbf{p}} = \begin{pmatrix} \sin \theta_p \\ 0 \\ \cos \theta_p \end{pmatrix} \tag{8}$$

Then, the unit vector of the C≡N bond, $\widehat{\mathbf{CN}}$, which makes an angle of $\Delta\theta = 10°$ with $\hat{\mathbf{p}}$ can be generally expressed as follows,

$$\widehat{\mathbf{CN}} = \begin{pmatrix} \cos \theta_p \sin \Delta\theta \cos \phi + \sin \theta_p \cos \Delta\theta \\ \sin \Delta\theta \sin \phi \\ -\sin \theta_p \sin \Delta\theta \cos \phi + \cos \theta_p \cos \Delta\theta \end{pmatrix} \tag{9}$$

where ϕ is the angle corresponding to the direction in which $\widehat{\mathbf{CN}}$ deviates from $\hat{\mathbf{p}}$ ($0 \le \phi < 360°$, see Figure 6 and the Supporting Information). The z-component in eq 9 is cos θ_{CN}. From eq 9, the error $\Delta\langle \cos^2 \theta_p \rangle$ was estimated (see Supporting Information for details):

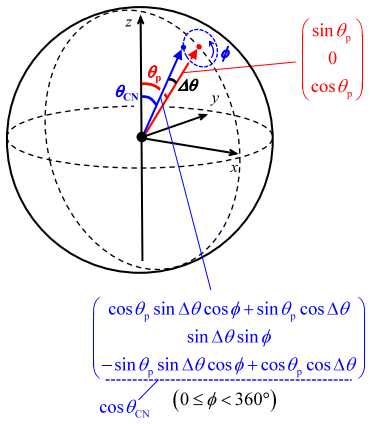

Figure 6. PDM and C≡N bond unit vectors, $\hat{\mathbf{p}}$ (red) and $\widehat{\mathbf{CN}}$ (blue), respectively, with an angle of $\Delta\theta$ between them.

$$\begin{aligned} \Delta\langle \cos^2 \theta_p \rangle &\equiv \langle \cos^2 \theta_{CN} \rangle - \langle \cos^2 \theta_p \rangle \\ &= \frac{1}{2}[1 - 3\langle \cos^2 \theta_p \rangle]\sin^2 \Delta\theta \\ &\simeq \frac{1}{2}[1 - 3\langle \cos^2 \theta_{CN} \rangle]\sin^2 \Delta\theta \\ &= \frac{1}{2}[1 - 3 \times 0.28] \times 0.030 \\ &= 0.0024 \end{aligned} \tag{10}$$

where we assume that ϕ is isotropic and independent of θ_p and that the second-order error is negligible, which are valid when $\Delta\theta$ is as small as 10°. This obtained error is sufficiently small to justify our approximation that $\langle \cos^2 \theta_{CN} \rangle$ is equal to $\langle \cos^2 \theta_p \rangle$.

Based on the above result, we assumed that $\langle \cos^2 \theta_{CN} \rangle$ and $\langle \cos^2 \theta_p \rangle$ were equivalent and calculated the variance of cos θ_p, $V_{\cos \theta_p}$, using eq 1; $V_{\cos \theta_p} = 0.28$. With values for the average and variance, $\langle \cos \theta_p \rangle = 0.045$ and $V_{\cos \theta_p} = 0.28$, respectively, the angular distribution of the PDMs in vacuum-deposited mCPCN films can be determined, and this will be plotted and discussed in Section 3.5.

3.4. Relationship Between the Variance and Angular Distribution. Before plotting and discussing the PDM angular distribution in the mCPCN films, we now discuss the relationship between the variance and angular distribution for some typical hypothetical cases to understand the importance of the variance. We consider three cases, (i)−(iii), that are each characterized by $\langle \cos \theta_p \rangle = 0$: (i) the PDM orientation is completely random with $V_{\cos \theta_p} = 0.33$ ($S = 0$), (ii) the PDM orientation is moderately horizontal with $V_{\cos \theta_p} = 0.15$ ($S = -0.28$), and (iii) the PDM orientation is moderately vertical with $V_{\cos \theta_p} = 0.50$ ($S = +0.25$). In case (i), in which the orientation is completely random, the distribution of cos θ_p corresponds to equipartition (Figure 7a, gray line), and the angular distribution of θ_p is a sine curve (Figure 7b). In this case, $V_{\cos \theta_p}$ must, statistically, to be 0.33. Next, in case (ii), in which the orientation is moderately horizontal, the distribution of cos θ_p can be uniquely plotted from the values of the average (0) and variance (0.15) by assuming a normal distribution (Figure 7a, green line). The angular distribution of θ_p for this case is also plotted in Figure 7b, where the population of the horizontal orientation is higher while those

https://doi.org/10.1021/acs.jpcc.3c08315
J. Phys. Chem. C 2024, 128, 6072−6079

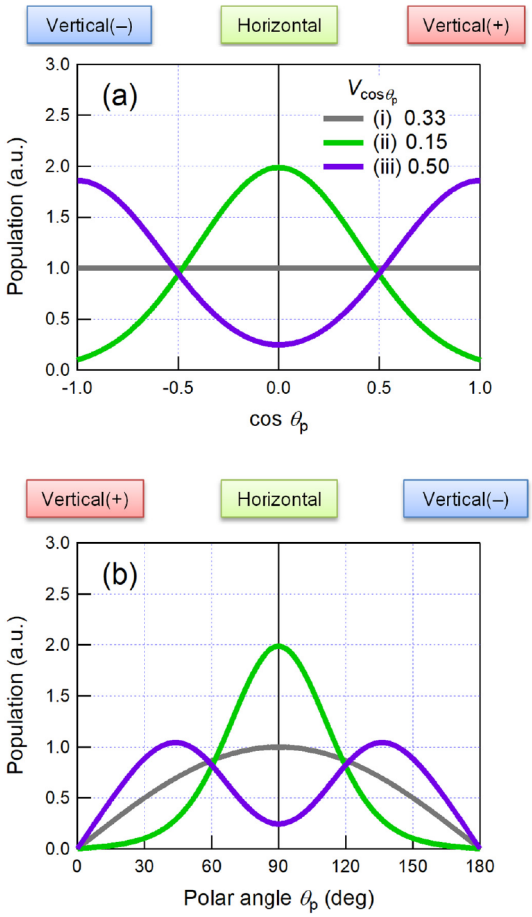

Figure 7. (a) Distributions of cos θ_p and (b) angular distributions of θ_p assuming a normal distribution of cos θ_p, when $\langle\cos\theta_p\rangle = 0$ and $V_{\cos\theta_p}$ = (i) 0.33, (ii) 0.15, and (iii) 0.50.

of the vertical(+) (vertical with top direction) and vertical(−) (vertical with bottom direction) orientations are lower compared to those for case (i). Then, in case of (iii), in which the orientation is moderately vertical, the distribution of cos θ_p can be plotted from the values of the average (0) and variance (0.50) by assuming that it is a sum of two symmetric normal distributions (Figure 7a, purple line). The angular distribution of θ_p for this case is also plotted in Figure 7b, where the populations of the vertical(+) and vertical(−) orientations are higher while that of the horizontal orientation is lower compared to those for case (i). In this case, the PDM orientation is moderately vertical, but the contributions of the vertical(+) and vertical(−) orientations to $\langle\cos\theta_p\rangle$ are strongly canceled each other out, with the result that $\langle\cos\theta_p\rangle = 0$.

As demonstrated by these three typical cases, even when $\langle\cos\theta_p\rangle$ takes the same value, the angular distribution can be quite different depending on $V_{\cos\theta_p}$. In particular, the difference between cases (ii) $V_{\cos\theta_p} < 0.33$ and (iii) $V_{\cos\theta_p} > 0.33$ is important because the plausible mechanism of formation and cancellation of SOP is expected to be different depending on it. In case (ii), $|\cos\theta_p|$ for most of the PDMs is small, and $\langle\cos\theta_p\rangle$ is weakly canceled, whereas in case (iii), $|\cos\theta_p|$ for most of the PDMs is large, but $\langle\cos\theta_p\rangle$ is strongly canceled, as schematically shown in Figure 8.

3.5. Angular Distribution of the PDMs of mCPCN.

Based on the results of $\langle\cos\theta_p\rangle = 0.045$ and $V_{\cos\theta_p} = 0.28$ for

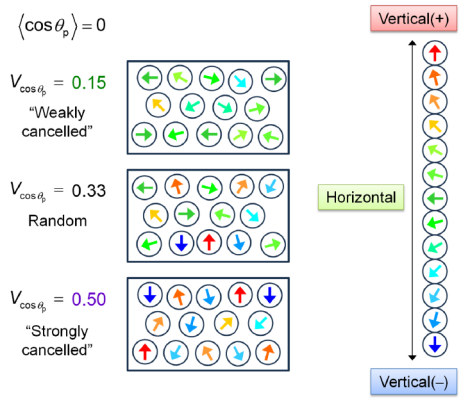

Figure 8. Schematic illustration of PDM orientation depending on $V_{\cos\theta_p}$ when $\langle\cos\theta_p\rangle = 0$.

the mCPCN films, the distribution of cos θ_p was uniquely plotted assuming a normal distribution (Figure 9a). Because $\langle\cos\theta_p\rangle$ is small and $V_{\cos\theta_p}$ is less than 0.33, the distribution is similar to that of case (ii) shown in Figure 7a, although the degree of horizontal orientation is more moderate. The

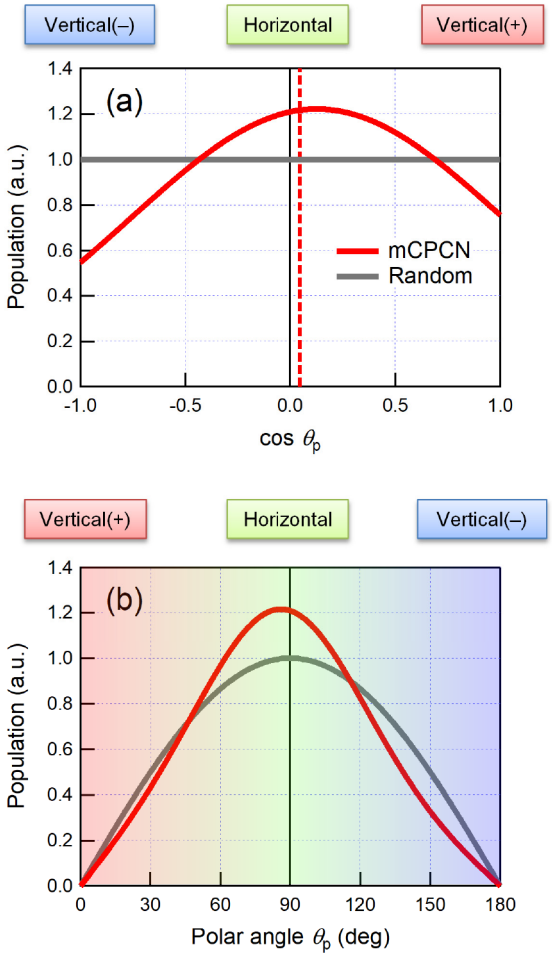

Figure 9. (a) Distributions of cos θ_p and (b) angular distributions of θ_p for the PDMs of the mCPCN molecules in vacuum-deposited films assuming a normal distribution of cos θ_p. For comparison, those for the random orientation are also shown. The red dashed line in (a) indicates the average value of cos θ_p.

https://doi.org/10.1021/acs.jpcc.3c08315
J. Phys. Chem. C 2024, 128, 6072−6079

distribution peak is from the center to a positive value owing to the positive value of $\langle \cos \theta_p \rangle$. From this result, the angular distribution of θ_p was also plotted (Figure 9b). Compared to the distribution for the random orientation, the populations of the vertical(+) and vertical(−) orientations are slightly lower, and the population of the horizontal orientation is higher by just the same amount, indicating that the orientation of the PDMs of the mCPCN molecules in the film is slightly horizontal overall ($S = -0.08$). The shift of the distribution peak from the center is very minor, but this very slight deviation of the distribution is the origin of the large SOP observed in vacuum-deposited mCPCN films.

The finding that $V_{\cos \theta_p} = 0.28 < 0.33$ for mCPCN films excludes the possibility that the vertical components of the PDMs are strongly canceled out as in case (iii). The PDM orientation (and C≡N bond orientation) is almost random and slightly horizontal overall, and the vertical component of the PDMs is not completely canceled out but remains positive. This experimental result supports a previously published simulation result,[30] which showed that strong dipole−dipole interactions are not the principal origin of the large SOPs of commonly used OLED materials, because strong dipole−dipole interactions would lead to a PDM orientation distribution similar to that of case (iii). The large SOP of mCPCN films is the result of just a slight deviation in the positive direction of the angular distribution of the PDMs from the random orientation distribution. This slight deviation can be regarded as a perturbation of the PDM orientation from the random orientation, which occurs because of the molecular shape anisotropy and polarity of the mCPCN molecule. It is noteworthy that a slight perturbative deviation of the angular distribution as seen in Figure 9b can result in very large SOP in OLED films.

Although our focus was mCPCN in this study, the same methods can be applied to OLED materials that satisfy a condition; the PDM of the molecule should be well along the TDM (dipole derivative) of an IR-active vibrational mode. Although the methods cannot be applied to materials that do not satisfy this condition (for example, mCP), there are some other OLED materials that satisfy it (for example, Ir(ppy)$_2$(acac)). In future, we plan to analyze the PDM angular distributions in vacuum-deposited films of other OLED materials and investigate the dependence of the angular distribution on the material. This should allow us to further understand the formation mechanism of SOP observed in commonly used OLED materials.

4. CONCLUSIONS

In this study, we analyzed the angular distribution of the PDMs in vacuum-deposited films of mCPCN, which is a commonly used host material in high-performance OLEDs. The average of cos θ_p, $\langle \cos \theta_p \rangle$, was estimated from the results of the chemical calculations, Kelvin probe measurements, XRR measurements, and impedance measurements. Then, based on the IR absorption measurements, the variance of cos θ_p, $V_{\cos \theta_p}$, was estimated by taking advantage of the fact that $\langle \cos^2 \theta_{CN} \rangle$ can be assumed to be approximately equal to $\langle \cos^2 \theta_p \rangle$. Having both $\langle \cos \theta_p \rangle$ and $V_{\cos \theta_p}$, we were able to uniquely plot the angular distribution of the PDMs assuming a normal distribution of cos θ_p. We found that the large SOP of mCPCN films arose owing to only a slight positive deviation of the PDM angular distribution from the random orientation distribution. Thus, these results provide visualization of the fact that such a slight deviation can produce large SOP in films of commonly used OLED materials. Our methods for the analysis of $\langle \cos \theta_p \rangle$ and $V_{\cos \theta_p}$ can be considered as general methods for determining the angular distributions of PDMs of commonly used OLED materials whose PDM is well along the TDM of an IR-active vibrational mode, and we believe that the use of these methods will lead to further advances in our understanding of the formation mechanism of the large SOP observed in many types of OLED films.

■ ASSOCIATED CONTENT

Supporting Information

The Supporting Information is available free of charge at https://pubs.acs.org/doi/10.1021/acs.jpcc.3c08315.

Derivation of cos θ_{CN}; estimation of the error $\Delta\langle \cos^2 \theta_p \rangle$; unit vectors (Figure S1) (PDF)

■ AUTHOR INFORMATION

Corresponding Author

Daisuke Yokoyama − *Department of Organic Materials Science, Yamagata University, Yonezawa, Yamagata 992-8510, Japan; Research Center for Organic Electronics (ROEL), Yamagata University, Yonezawa, Yamagata 992-8510, Japan;* orcid.org/0000-0001-5484-7213; Email: d_yokoyama@yz.yamagata-u.ac.jp

Authors

Yuro Yagi − *Department of Organic Materials Science, Yamagata University, Yonezawa, Yamagata 992-8510, Japan*

Yutaka Noguchi − *School of Science & Technology, Meiji University, Kawasaki, Kanagawa 214-8571, Japan;* orcid.org/0000-0002-1108-994X

Complete contact information is available at: https://pubs.acs.org/10.1021/acs.jpcc.3c08315

Notes

The authors declare no competing financial interest.

■ ACKNOWLEDGMENTS

The authors thank Prof. Hisahiro Sasabe and Mr. Naoto Yoshida at Yamagata University for helpful discussions. The DFT computations were performed using the facilities of Research Center for Computational Science, Okazaki, Japan (Project: 23-IMS-C145).

■ REFERENCES

(1) Yokoyama, D. Molecular Orientation in Small-Molecule Organic Light-Emitting Diodes. *J. Mater. Chem.* **2011**, *21*, 19187−19202.

(2) Brütting, W.; Frischeisen, J.; Schmidt, T. D.; Scholz, B. J.; Mayr, C. Device Efficiency of Organic Light-Emitting Diodes: Progress by Improved Light Outcoupling. *Phys. Status Solidi A* **2013**, *210*, 44−65.

(3) Schmidt, T. D.; Lampe, T.; Sylvinson, M. R. D.; Djurovich, P. I.; Thompson, M. E.; Brütting, W. Emitter Orientation as a Key Parameter in Organic Light-Emitting Diodes. *Phys. Rev. Appl.* **2017**, *8*, 037001.

(4) Kim, K.-H.; Kim, J.-J. Origin and Control of Orientation of Phosphorescent and TADF Dyes for High-Efficiency OLEDs. *Adv. Mater.* **2018**, *30*, 1705600.

(5) Bagchi, K.; Ediger, M. D. Controlling Structure and Properties of Vapor-Deposited Glasses of Organic Semiconductors: Recent Advances and Challenges. *J. Phys. Chem. Lett.* **2020**, *11*, 6935−6945.

(6) Noguchi, Y.; Brütting, W.; Ishii, H. Spontaneous Orientation Polarization in Organic Light-Emitting Diodes. *Jpn. J. Appl. Phys.* **2019**, *58*, SF0801.
(7) Noguchi, Y.; Tanaka, Y.; Ishii, H.; Brütting, W. Understanding Spontaneous Orientation Polarization of Amorphous Organic Semiconducting Films and Its Application to Devices. *Synth. Met.* **2022**, *288*, 117101.
(8) Ito, E.; Washizu, Y.; Hayashi, N.; Ishii, H.; Matsuie, N.; Tsuboi, K.; Ouchi, Y.; Harima, Y.; Yamashita, K.; Seki, K. Spontaneous Buildup of Giant Surface Potential by Vacuum Deposition of Alq_3 and Its Removal by Visible Light Irradiation. *J. Appl. Phys.* **2002**, *92*, 7306−7310.
(9) Osada, K.; Goushi, K.; Kaji, H.; Adachi, C.; Ishii, H.; Noguchi, Y. Observation of Spontaneous Orientation Polarization in Evaporated Films of Organic Light-Emitting Diode Materials. *Org. Electron.* **2018**, *58*, 313−317.
(10) Hofmann, A.; Schmid, M.; Brütting, W. The Many Facets of Molecular Orientation in Organic Optoelectronics. *Adv. Optical Mater.* **2021**, *9*, 2101004.
(11) Noguchi, Y.; Sato, N.; Miyazaki, Y.; Nakayama, Y.; Ishii, H. Higher Resistance to Hole Injection and Electric Field Distribution in Organic Light-Emitting Diodes with Copper Phthalocyanine Interlayer. *Jpn. J. Appl. Phys.* **2010**, *49*, 01AA01.
(12) Noguchi, Y.; Lim, H.; Isoshima, T.; Ito, E.; Hara, M.; Chin, W. W.; Han, J. W.; Kinjo, H.; Ozawa, Y.; Nakayama, Y.; et al. Influence of the Direction of Spontaneous Orientation Polarization on the Charge Injection Properties of Organic Light-Emitting Diodes. *Appl. Phys. Lett.* **2013**, *102* (20), 203306.
(13) Altazin, S.; Züfle, S.; Knapp, E.; Kirsch, C.; Schmidt, T. D.; Jäger, L.; Noguchi, Y.; Brütting, W.; Ruhstaller, B. Simulation of OLEDs with a Polar Electron Transport Layer. *Org. Electron.* **2016**, *39*, 244−249.
(14) Berleb, S.; Brütting, W.; Paasch, G. Interfacial Charges and Electric Field Distribution in Organic Hetero-Layer Light-Emitting Devices. *Org. Electron.* **2000**, *1*, 41−47.
(15) Noguchi, Y.; Miyazaki, Y.; Tanaka, Y.; Sato, N.; Nakayama, Y.; Schmidt, T. D.; Brütting, W.; Ishii, H. Charge Accumulation at Organic Semiconductor Interfaces Due to a Permanent Dipole Moment and Its Orientational Order in Bilayer Devices. *J. Appl. Phys.* **2012**, *111* (11), 114508.
(16) Bangsund, J. S.; Van Sambeek, J. R.; Concannon, N. M.; Holmes, R. J. Sub−turn-on exciton quenching due to molecular orientation and polarization in organic light-emitting devices. *Sci. Adv.* **2020**, *6* (32), No. eabb2659.
(17) Pakhomenko, E.; He, S.; Holmes, R. J. Understanding and Engineering Spontaneous Orientation Polarization in Organic Light-Emitting Devices. *Chem. Phys. Rev.* **2023**, *4* (2), 021308.
(18) Kondakov, D. Y.; Sandifer, J. R.; Tang, C. W.; Young, R. H. Nonradiative Recombination Centers and Electrical Aging of Organic Light-Emitting Diodes: Direct Connection Between Accumulation of Trapped Charge and Luminance Loss. *J. Appl. Phys.* **2003**, *93*, 1108−1119.
(19) Jarikov, V. V.; Kondakov, D. Y. Studies of the Degradation Mechanism of Organic Light-Emitting Diodes Based on Tris(8-quinolinolate)aluminum Alq and 2-*Tert*-butyl-9,10-di(2-naphthyl)-anthracene TBADN. *J. Appl. Phys.* **2009**, *105* (3), 034905.
(20) Noguchi, Y.; Kim, H.-J.; Ishino, R.; Goushi, K.; Adachi, C.; Nakayama, Y.; Ishii, H. Charge Carrier Dynamics and Degradation Phenomena in Organic Light-Emitting Diodes Doped by a Thermally Activated Delayed Fluorescence Emitter. *Org. Electron.* **2015**, *17*, 184−191.
(21) Schmidt, T. D.; Jäger, L.; Noguchi, Y.; Ishii, H.; Brütting, W. Analyzing Degradation Effects of Organic Light-Emitting Diodes via Transient Optical and Electrical Measurements. *J. Appl. Phys.* **2015**, *117* (21), 215502.
(22) Afolayan, E. O.; Dursun, I.; Lang, C.; Pakhomenko, E.; Kondakova, M.; Boroson, M.; Hickner, M.; Holmes, R. J.; Giebink, N. C. Reducing Spontaneous Orientational Polarization via Semiconductor Dilution Improves OLED Efficiency and Lifetime. *Phys. Rev. Appl.* **2022**, *17* (5), L051002.
(23) Isoshima, T.; Okabayashi, Y.; Ito, E.; Hara, M.; Chin, W. W.; Han, J. W. Negative Giant Surface Potential of Vacuum-Evaporated Tris(7-propyl-8-hydroxyquinolinolato)aluminum(III) $[Al(7\text{-}Prq)_3]$ film. *Org. Electron.* **2013**, *14*, 1988−1991.
(24) Bagchi, K.; Jackson, N. E.; Gujral, A.; Huang, C.; Toney, M. F.; Yu, L.; De Pablo, J. J.; Ediger, M. D. Origin of Anisotropic Molecular Packing in Vapor-Deposited Alq3 Glasses. *J. Phys. Chem. Lett.* **2019**, *10*, 164−170.
(25) Schmid, M.; Harms, K.; Degitz, C.; Morgenstern, T.; Hofmann, A.; Friederich, P.; Johannes, H.-H.; Wenzel, W.; Kowalsky, W.; Brütting, W. Optical and Electrical Measurements Reveal the Orientation Mechanism of Homoleptic Iridium-Carbene Complexes. *ACS Appl. Mater. Interfaces* **2020**, *12*, 51709−51718.
(26) Morgenstern, T.; Schmid, M.; Hofmann, A.; Bierling, M.; Jäger, L.; Brütting, W. Correlating Optical and Electrical Dipole Moments to Pinpoint Phosphorescent Dye Alignment in Organic Light-Emitting Diodes. *ACS Appl. Mater. Interfaces* **2018**, *10*, 31541−31551.
(27) Noguchi, N.; Osada, K.; Ninomiya, K.; Gunawardana, H. D. C. N.; Koswattage, K. R.; Ishii, H. Influence of Intermolecular Interactions on the Formation of Spontaneous Orientation Polarization in Organic Semiconducting Films. *J. Soc. Inf. Display* **2021**, *29*, 29−37.
(28) Tanaka, M.; Auffray, M.; Nakanotani, H.; Adachi, C. Spontaneous Formation of Metastable Orientation with Well-Organized Permanent Dipole Moment in Organic Glassy Films. *Nat. Mater.* **2022**, *21*, 819−825.
(29) Ediger, M. D.; de Pablo, J.; Yu, L. Anisotropic Vapor-Deposited Glasses: Hybrid Organic Solids. *Acc. Chem. Res.* **2019**, *52*, 407−414.
(30) Friederich, P.; Rodin, V.; von Wrochem, F.; Wenzel, W. Built-In Potentials Induced by Molecular Order in Amorphous Organic Thin Films. *ACS Appl. Mater. Interfaces* **2018**, *10*, 1881−1887.
(31) Lin, M.-S.; Yang, S.-J.; Chang, H.-W.; Huang, Y.-H.; Tsai, Y.-T.; Wu, C.-C.; Chou, S. H.; Mondal, E.; Wong, K.-T. Incorporation of a CN Group into mCP: A New Bipolar Host Material for Highly Efficient Blue and White Electrophosphorescent Devices. *J. Mater. Chem.* **2012**, *22*, 16114−16120.
(32) Sarma, M.; Tsai, W.-L.; Lee, W.-K.; Chi, Y.; Wu, C.-C.; Liu, S.-H.; Chou, P.-T.; Wong, K.-T. Anomalously Long-Lasting Blue PhOLED Featuring Phenyl-Pyrimidine Cyclometalated Iridium Emitter. *Chem* **2017**, *3*, 461−476.
(33) Zeng, W.; Lai, H.-Y.; Lee, W.-K.; Jiao, M.; Shiu, Y.-J.; Zhong, C.; Gong, S.; Zhou, T.; Xie, G.; Sarma, M.; et al.etal. Achieving Nearly 30% External Quantum Efficiency for Orange−Red Organic Light Emitting Diodes by Employing Thermally Activated Delayed Fluorescence Emitters Composed of 1,8-Naphthalimide-Acridine Hybrids. *Adv. Mater.* **2018**, *30*, 1704961.
(34) Sasabe, H.; Chikayasu, Y.; Ohisa, S.; Arai, H.; Ohsawa, T.; Komatsu, R.; Watanabe, Y.; Yokoyama, D.; Kido, J. Molecular Orientations of Delayed Fluorescent Emitters in a Series of Carbazole-Based Host Materials. *Front. Chem.* **2020**, *8*, 427.
(35) Chen, Y.-K.; Jayakumar, J.; Hsieh, C.-M.; Wu, T.-L.; Liao, C.-C.; Pandidurai, J.; Ko, C.-L.; Hung, W.-Y.; Cheng, C.-H. Triarylamine-Pyridine-Carbonitriles for Organic Light-Emitting Devices with EQE Nearly 40%. *Adv. Mater.* **2021**, *33*, 2008032.
(36) Sakai, Y.; Shibata, M.; Yokoyama, D. Simple Model-Free Estimation of Orientation Order Parameters of Vacuum-Deposited and Spin-Coated Amorphous Films Used in Organic Light-Emitting Diodes. *Appl. Phys. Express* **2015**, *8* (9), 096601.
(37) Sukegawa, Y.; Sakai, Y.; Yokoyama, D. Model-Free Analysis of Molecular Orientation in Amorphous Organic Semiconductor Films for Understanding Its Formation Dynamics: Methods and Systematic Investigation. *Org. Electron.* **2022**, *100*, 106377.

https://doi.org/10.1021/acs.jpcc.3c08315
J. Phys. Chem. C 2024, 128, 6072−6079